A Baseline Study of Oxygen Saturation in Parafoveal Vessels Using Visible Light Optical Coherence Tomography

Jingyu Wang[1], Weiye Song[2,3], Natalie Sadlak[3], Marissa G. Fiorello[3], Manishi Desai[3] and Ji Yi[1,4*]

[1] Department of Ophthalmology, School of Medicine, Johns Hopkins University, Baltimore, MD, United States, [2] School of Mechanical Engineering, Shandong University, Jinan, China, [3] Department of Ophthalmology, Boston Medical Center, Boston, MA, United States, [4] Department of Biomedical Engineering, Johns Hopkins University, Baltimore, MD, United States

The retinal macula is at the center of our visual field, and thus pathological damage in the macula significantly impacts an individual's quality of life. The parafoveal vessels form the inner retina provide oxygen perfusion, and the measurement of parafoveal oxygen saturation (sO_2) can evaluate macular metabolism and provide pathophysiological insight. In this paper, for the first time, we present a baseline study of microvascular oxygen saturation (sO_2) in perifoveal macular region using visible light optical coherence tomography (VIS-OCT) on normal eyes. The arterial and venous sO_2 from all eyes was 92.1 ± 7.1 (vol %) and 48.4 ± 5.0 (vol %) (mean $\pm$ SD), respectively. Arteriovenous sO_2 difference was 43.8 ± 9.5 (vol %). Marginal correlation was found between venous sO_2 and intraocular pressure (IOP) among eyes. No significant correlation was found between sO_2 and vessel topological features, including length, diameter, and distance to fovea. This baseline study could serve as a benchmark for the future sO_2 investigation of retinal macular pathologies.

Keywords: visible light optical coherence tomography, retinal oximetry, baseline study, parafoveal vessels, segmentation

INTRODUCTION

Oxygen supply supports the metabolism of the human retina, and abnormal oxygen perfusion is associated with various retinal conditions leading to vision damage and blindness, including glaucoma, age-related macular degeneration, diabetic retinopathy, and vascular occlusions (1). Therefore, the measurement of blood oxygen saturation within the retinal circulation is not only essential to understanding the physiopathology of retinal diseases, but also can play important role for detection and monitoring.

Label-free optical retinal oximetry harnesses the oxygen-dependent spectral contrast of endogenous hemoglobin to non-invasively measure oxygen saturation quantitatively in the human retina (2–6). A fundus camera based multi-wavelength oximetry has been previously reported in several clinical studies on retinal conditions (7). However, the technique lacks depth resolution, and the measurement is complicated by the reflections from vessel surface. So far, only readings from large vessels in the peri-papillary region have been reported.

Visible light optical coherence tomography (VIS-OCT) is a recent development that provides the necessary 3D imaging capacity to eliminate confounding signals from other retinal layers and the choroid (8–12). The much stronger absorption in visible light range than conventional near infrared light (8), in conjunction with 3D segmentation of retinal blood vessels, permits reliable spatio-spectral analysis for microvascular retinal oximetry (11). By combining OCT angiography, capillary oximetry in the human retina has been recently reported which is a significant technical contribution. The initial report of *in vivo* oximetry using VIS-OCT was introduced in 2011 (13), then VIS-OCT oximetry was applied in rat's retina in 2013 (8). After several years of development, the technique has been successfully demonstrated in human retina in pathological cases for clinical research, including glaucoma, retinal ischemia, diabetic retinopathy (DR), central retinal vein occlusion (CRVO) and sickle cell retinopathy (SCR) (14–16).

Being responsible for the central vision field and acuity, macular region contains >30% of the total ganglion cells in the whole retina (17) in addition to being enriched with cone photoreceptors. The quantification of macular vascular sO_2 has important implications for macular retinal function and metabolism. However, existing reports so far have evaluated the sO_2 of large retinal vessel around the optic nerve head (ONH) (4, 18–20). Due to lack of resolution in fundus-based 2D oximetry, macular region vascular sO_2 has not been sufficiently studied before. In this study, for the first time, we report a baseline study of sO_2 of parafoveal arterioles and venules. We analyze the association of the arterial and venous sO_2 with ophthalmic exam, and OCT macular and ONH scans. The result will serve as an important reference for the future comparison with pathological data.

MATERIALS AND METHODS

Human Subjects

This study was conducted at Boston Medical Center, whose Institutional Review Board reviewed and approved the study. The study was compliant with the Health Insurance Portability and Accountability Act and adhered to the tenets of the Declaration of Helsinki. Written informed consent was obtained from all subjects before participation. Healthy subjects were recruited through the Boston Medical Center Optometry clinics. Cataracts were evaluated using the Lens Opacification System II based upon color and opalescence (21). The system uses a 4-point grading system with increasing number consistent with increasing maturity. Severe cataracts graded more than 2+ were excluded. All the subjects went through a regular ophthalmic examination including refractive error, tonometry for intraocular pressure (IOP), stereoscopic optic disc assessment, as well as clinical OCT scans of optic nerve head (ONH) and macula by Zeiss Cirrus OCT device. The OCT thickness of circumpapillary retinal nerve fiber layer (cpRNFL) and macular ganglion cell complex (GCC: ganglion cell layer + inner plexiform layer) were recorded, as well as cup to disc ratio (CDR). Dual-channel VIS-OCT was performed subsequently, and parafoveal vessel oxygen

saturation (sO_2) were quantified by post-processing. The subjects were imaged by trained technicians.
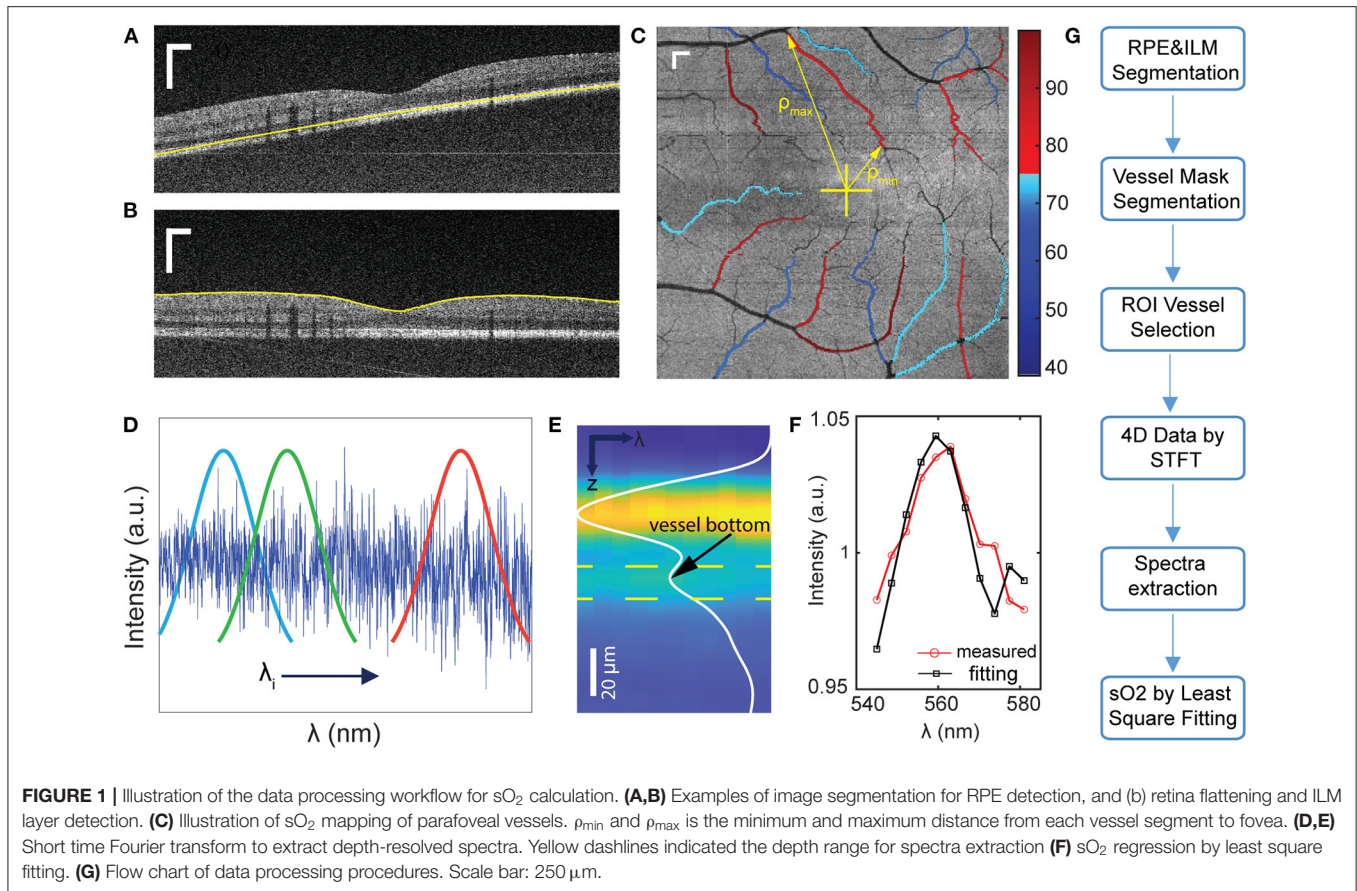
Study Device and Method

The detailed setup of self-built vis-OCT system can be referenced in our previous publication (22). The pattern of raster scanning was 512×256 pixels and signals were received by a line camera with a line rate of 50 kHz and an exposure time of 19.1 μs. The image field of view (FOV) was 5×5 mm taking 2.62 s to acquire. The laser power on the cornea was <0.25 mW which is safe under the ANSI standard of ophthalmic instrument. After acquiring the raw interference signals, 3D data vis-OCT was generated by removing DC, converting the signals in k-space, digitally compensating the dispersion, and performing Fourier transform to prepare for later retinal boundary segmentation.

Image Segmentation

We first detected the retinal pigmented epithelium (RPE) layer as the outer retina boundary. We blurred each B-scan by the Gaussian filter with a standard deviation of 7, then identified the RPE depth by detecting the maximum intensities along the A-line. Several factors can influence the accuracy of detection results, including the vessel shadows, high intensities in the retinal nerve fiber layer (RNFL) and system noise. To address these factors, we performed a correction by using a two-step outlier detection and replacement, as detailed below.

We used a third-order polynomial to fit the detected RPE curve within each B-scan, then calculated the difference between the fitted and detected curves. The mean and standard deviation (SD) of the difference were obtained. When the difference is outside the range of mean $\pm 1.8 \times$ SD, this point on the detected RPE curve was considered as an outlier and deleted. Then we used the remaining points to generate the new polynomial fitting curve to replace the outliers and iterated this process until no outlier was found. We also calculated the coefficient of variation (COV) of each final fitted curve within each B-scan. After processing all B-scans, we obtained a COV curve over all B-scans, then we performed the outlier detection in the COV curve using the same standard to find the outliers. The values of COV of each fitting curve in adjacent images is expected to be similar. If the COV of two adjacent curves changed greatly in some frames, that usually mean the segmentation failed, and we discarded the outlier curve and used the previous curve to replace it. After this method, the retina was flattened based on accurate RPE labeling as shown in **Figures 1A,B**. In the next step, the inner limiting membrane (ILM) can be easily determined by the greatest gradient changes of intensities in the region above the RPE (**Figure 1B**).

We averaged the signals 20 pixels above RPE to generate the *en face* image. The vessel mask was obtained by binarizing the *en face* image with an adaptive threshold (23). Based on this vessel mask, we manually selected the vessel in the region of interest (ROI) as illustrated in **Figure 1C**. We considered the vessels branching from grandparents, to parents, and to children. Because of the strong blood absorption in VIS-OCT, the large grandparent vessels can be challenging to locate the vessel bottom and lack regional specification. Therefore, we focused on

FIGURE 1 | Illustration of the data processing workflow for sO$_2$ calculation. **(A,B)** Examples of image segmentation for RPE detection, and (b) retina flattening and ILM layer detection. **(C)** Illustration of sO$_2$ mapping of parafoveal vessels. ρ_{min} and ρ_{max} is the minimum and maximum distance from each vessel segment to fovea. **(D,E)** Short time Fourier transform to extract depth-resolved spectra. Yellow dashlines indicated the depth range for spectra extraction **(F)** sO$_2$ regression by least square fitting. **(G)** Flow chart of data processing procedures. Scale bar: 250 μm.

smaller parafoveal vessels and stopped at major branching points. When the two vessels were intersecting, we avoided selecting the overlaying portions. Tiny children vessels were also neglected as the adaptive threshold algorithm failed to recognize them.

Oxygen Saturation Calculation

We generated the wavelength-dependent four-dimensional (4D) data I (x, y, z, λ) by the Short-time Fourier transform with 11 Gaussian windows sweeping the spectral interferogram (**Figure 1D**). We flatten all A-lines within each vessel ROI with respect to ILM and averaged all the A-lines of 4D data to generate the spectra in terms of depth I (z, λ) (**Figure 1E**). These spectra were then normalized by the averaged spectrum from non-vascular RNFL (22). To locate the vessel bottom, we averaged over λ and obtained an averaged A-line signal as the curve shown in **Figure 1E**. The location of the second reflective peak from ILM is identified as the vessel bottom. We then averaged the signals in the range of 5 pixels above and 10 pixels below the vessel bottom (area between the two yellow dash line in **Figure 1E**) in I (z, λ) to generate the single spectrum (**Figure 1F**).

Finally, we used a least square fitting on the extracted spectra to calculate the sO$_2$ of ROI vessels. The model and algorithm were clarified in our previous work (22).

$$I(sO_2|\lambda, z) = I_0(\lambda)\sqrt{R_0 r(\lambda)}e^{-[sO_2 \times \mu_{HbO_2}(\lambda) + (1-sO_2) \times \mu_{Hb}(\lambda)]z} \quad (1)$$

Where $I_0(\lambda)$ is the spectrum of light sources; R_0 is the reflectance of reference arm which is assumed to be constant; $r(\lambda)$ (dimensionless) is the reflectance at the vessel wall, modeled by a power law $r(\lambda) = A\lambda^{-\alpha}$, with A being a dimensionless constant and α modeling the decaying scattering spectrum from the vessel wall. Both A and α were included in the spectral fitting process. The detailed calculation for $r(\lambda)$ can be found in reference (22). For the parameters μ_{HbO_2} and μ_{Hb}, the optical attenuation coefficient μ is determined by the coefficients of absorption μ_a and scattering μ_s, where. $\mu(\lambda) = \mu_a(\lambda) + W\mu_s(\lambda)$. W is the scaling factor for the scattering coefficient which was 0.2 used here (8).

Vessel Topographic Feature Analysis

Several topographic features of manually selected vessels were quantified, including length (L), area (A), diameter (D), the minimum distance (ρ_{min}) and maximum distance (ρ_{max}) from fovea to vessel segments. Based on the *en face* images, the length and area were defined as the converted length of vessel centerline and area of whole vessel ROI segment. The diameter D was obtained by top and bottom of the vessels from averaged A-line signals. The accurate location of fovea was targeted manually by going through the 3D data combined with the *en face* image. With the known fovea location and selected vessel masks, we calculated ρ_{min} and ρ_{max} for each vessel segment.

TABLE 1 | Demographic information of subjects.

Subject numbers	10
Gender (female/male)	5/5
Eyes (OD/OS)	8/8
Ages (years)	61 ± 13.3
Race (White/AA/NA)	3/4/3
Ethnicity (Not Latino/Latino/NA)	7/2/1

AA, African American; NA, Not available.

TABLE 2 | Characteristics of ocular measurements from all eyes.

Characteristics	Mean (std)
Sphere (Diopter)	−0.50 (1.53)
Cylinder (Diopter)	0.77 (0.97)
IOP (mmHg)	15.4 (2.3)
CDR	0.33 (0.09)
GCC (μm)	78.0 (8.9)
cpRNFL (μm)	90.7 (10.0)
Superior cpRNFL (μm)	115.9 (14.0)
Nasal cpRNFL (μm)	70.3 (14.9)
Inferior cpRNFL (μm)	116.6 (17.4)
Temporal cpRNFL (μm)	61.6 (10.3)
AsO_2 (vol %)	92.1 (7.1)
VsO_2 (vol %)	48.4 (5.0)
A-V sO_2 (vol %)	43.8 (9.5)

Statistical Analysis

Statistical analysis was performed by MATLAB (The MathWorks, Inc.). Pearson's linear correlation coefficients were calculated between each pair of parameters, and unpaired parametric t-statistics were executed for the p-values. When the $p < 0.05$, the statistics was defined as the significant.

RESULTS

Fourteen healthy subjects in total were recruited in this study. Four subjects were excluded due to the failure of fixation, or low image quality. Fixation failures were due to significant eye movements during imaging where fovea was not present in the images, or the vessel locations were not recognizable. Lower image qualities caused the unsuccessful segmentation, leading to the failure of vessel selection and sO_2 calculation. Additional four eyes were excluded by the same criterion within the left ten subjects. The demographic information and the ophthalmic measurements are summarized in **Tables 1**, **2**. Sixteen eyes in total were used for the analysis. Nine eyes have mild Grade 1 cataract.

The sO_2 value for all arterioles and venules were first averaged within each eye, as shown in **Figure 2**. The mean arterial (AsO_2) and venous sO_2 (VsO_2) were 92.1 ± 7.1 (vol %) and 48.4 ± 5.0 (vol %) respectively. The mean arteriovenous sO_2 difference (A-V sO_2) was 43.8 ± 9.5 (vol %). The mean and standard deviation of
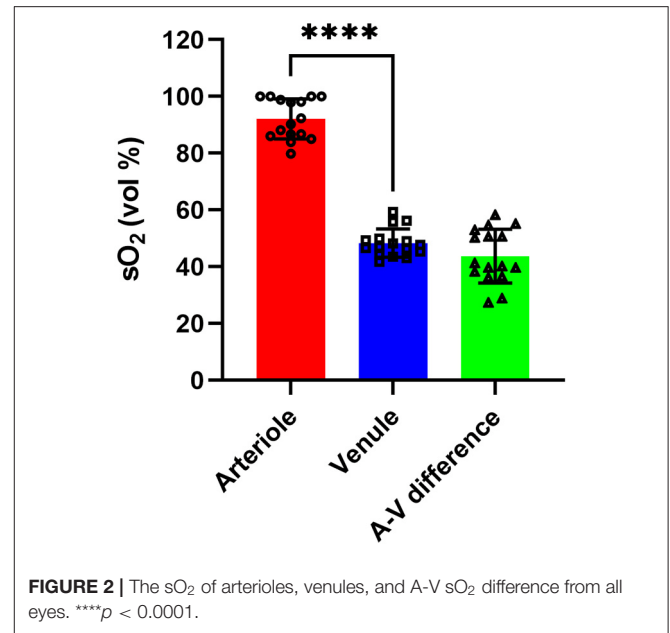

FIGURE 2 | The sO_2 of arterioles, venules, and A-V sO_2 difference from all eyes. ****$p < 0.0001$.

TABLE 3 | Correlation between clinical parameters and vessel sO_2 based on eyes.

Clinical Parameter	AsO_2		VsO_2		A-V sO_2	
	R	*p*	*r*	*p*	*r*	*p*
Sphere	−0.185	0.492	−0.368	0.160	0.055	0.838
Cylinder	0.195	0.524	0.184	0.546	0.045	0.884
IOP	0.253	0.344	−0.530	**0.035**	0.466	0.069
CDR	−0.173	0.521	0.514	**0.042**	−0.398	0.127
GCC	−0.007	0.980	−0.168	0.534	0.083	0.760
cpRNFL	−0.180	0.504	0.283	0.288	−0.282	0.291
Age	0.174	0.520	−0.546	**0.029**	0.414	0.110

Pearson's correlation was performed. Bold: p < 0.05.

vessel sO_2 for both arterioles and venules from all eyes are shown in **Supplementary Figure 3**.

Table 3 summarizes the correlation coefficients and p values between parafoveal AsO_2, VsO_2, A-V sO_2 and ophthalmic measurements including refractive errors, IOP, thickness of macular ganglion cell complex (GCC) and circumpapillary RNFL (cpRNFL). No significant correlation was found except between VsO_2 and IOP, cup/disk ratio (CDR) and age. **Figure 3** shows the correlation matrix map between sO_2 per eye and other ophthalmic parameters.

We further analyzed the correlation between sO_2 and vessel topographic parameters, which were in the **Supplementary Figures 1**, **2**. No significant correlation was found between sO_2 and vessel length (L), area (A), diameter (D), and the distance of ρ_{min} and ρ_{max}.

For the venules, A and L is significantly correlated as expected by geometry. The diameter positively correlated with the length and area of venules but with no significance. The minimum distance (ρ_{min}) has a negative correlation with length, area, and
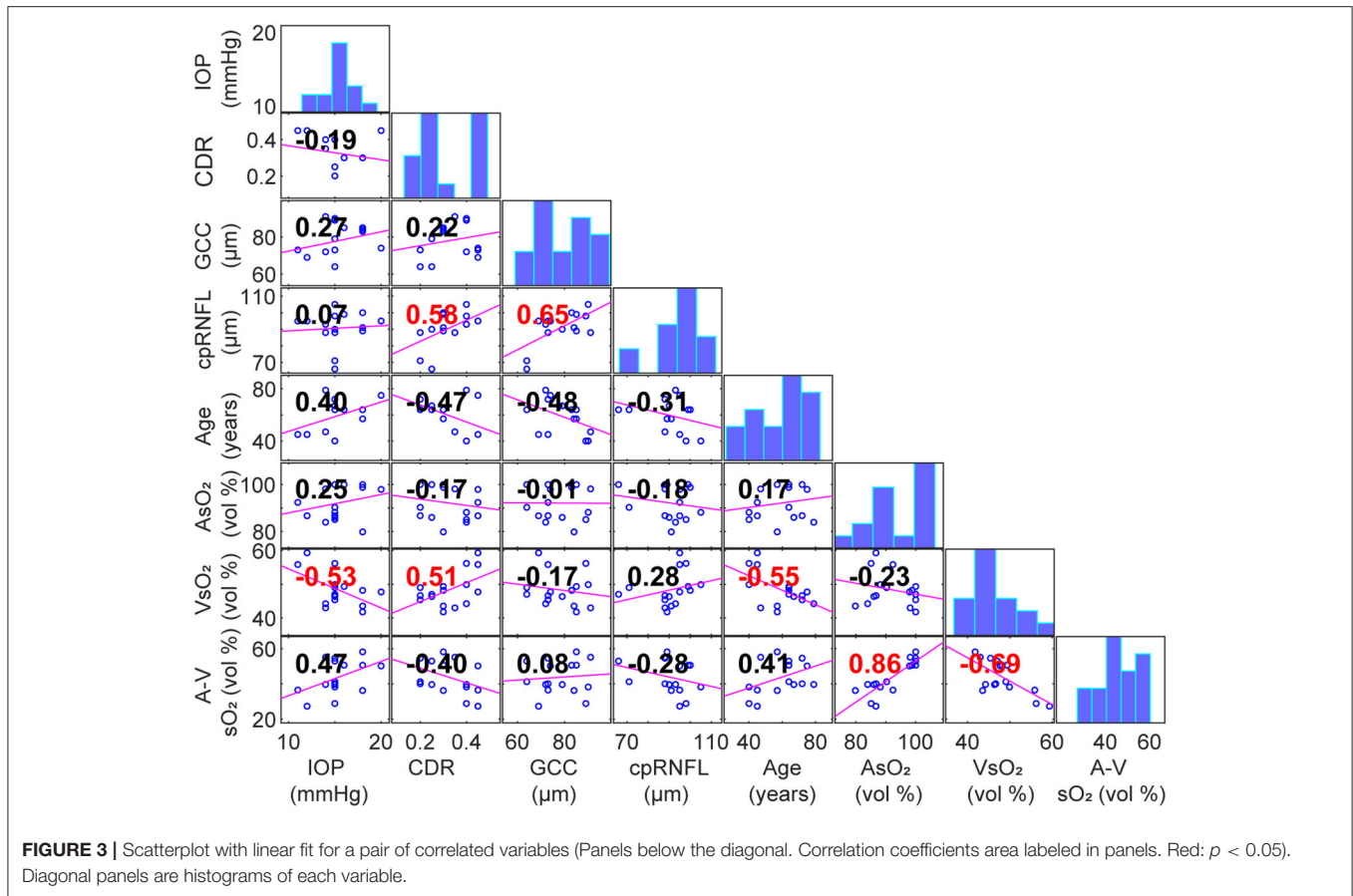
FIGURE 3 | Scatterplot with linear fit for a pair of correlated variables (Panels below the diagonal. Correlation coefficients area labeled in panels. Red: $p < 0.05$). Diagonal panels are histograms of each variable.

TABLE 4 | Vessel segment topographic parameters and sO_2 ($n = 57$ for arterioles, $n = 43$ for venules).

	Arterioles	Venules	p
L (mm)	1.19 ± 0.48	1.23 ± 0.42	0.709
A (10^{-3} mm^2)	32.5 ± 17.3	37.1 ± 16.6	0.184
D (µm)	24.8 ± 3.9	28.4 ± 3.2	**<0.001**
ρ_{min} (mm)	1.11 ± 0.39	1.16 ± 0.53	0.604
ρ_{max} (mm)	2.06 ± 0.51	2.26 ± 0.52	0.061
sO_2 (vol %)	91.0 ± 8.0	50.9 ± 8.8	**<0.001**

Two sample t-tests. Bold: $p < 0.05$.

diameter, but only has a significant dependency on the latter two. The maximum distance (ρ_{max}) has significant dependencies on all the other dimensions except diameter. For the arterioles, sO_2 has no significant correlation with topographic parameters. All the topographic parameters have significant correlation with each other, except for the ρ_{min} with length, area, and diameter.

Table 4 summarizes the topographic parameters and sO_2 values from all of arterious and venous segments. The AsO_2 and VsO_2 per segments are 91.0 ± 8.0 vol % ($n = 57$) and 50.9 ± 8.8 vol % ($n = 43$), and the diameter of venules is significantly larger than the arterioles' ($P < 0.001$). For the other parameters,

no significant difference was found. It is noted that diameters of both arterioles and venules are smaller than $40\,\mu m$.

DISCUSSION

In this paper, we report the first baseline study on parafoveal vessel oxygen saturation (sO_2) in healthy eyes. We quantified the topographic features of those vessels and found no significant correlation with sO_2 values. There is no significant correlation between sO_2 and cpRNFL, GCC thickness or refractive error. IOP moderately correlated with VsO_2; however, A-V sO_2 had no significant correlation with IOP. The significant association between VsO_2 and age and CDR was also found.

We found the negative correlation between VsO_2 and age in healthy subjects was significant, which is consistent with previous reports (24–26). We also found correlation between VsO_2 and IOP. There has been sparse literature investigating the association between VsO_2 and IOP. Liu et al. reported no association between IOP and sO_2 for the healthy children under 18 (27). However, there is a significant age difference in our study and thus it is difficult to compare. It is plausible that IOP was positively correlated to the age of people under 60 (28), leading to the negative correlation to the VsO_2. The positive association between VsO_2 and CDR was marginally significant, which can also be found in Vandewalle et al. (29). Despite above significant

correlation, we found no significant correlation between A-V sO$_2$ with age, IOP or CDR.

Compared to fundus-based or multi wavelength SLO oximetry (7, 30), VIS-OCT provides better depth resolution enabling precise segmentation from the bottom of the vessels, and avoids noise from other layers. The parafoveal vessels in this study have a modest diameter ranging from 20 to 30 μm where visible light may penetrate fully. Without the depth segmentation, the penetrated light would diffuse through other layers and create confounding factors in the fundus camera. This would also compromise the resolution and contrast and make macular oximetry challenging for 2D image-based methods. We also note that the relative smaller caliber of the parafoveal vessels may be better suited for VIS-OCT than larger peripapillary vessels around ONH, since the bottom of the vessels were easier to image than large vessels to create a strong reflectance signal.

While this is the first study of the parafoveal vessel sO$_2$ in normal human subjects using VIS-OCT oximetry, there are limitations worth noting. First, we had limited subject number in this pilot study. Therefore, we refrained from advanced multivariable statistical analysis and rather performed simple two-sample t-tests and Pearson's linear correlation. Marginal significances were found in some parameters stated above. A larger cohort would be needed in the future study to validate those significance by a multiple-variable analysis to incorporate variable interactions and other confounding factors. Second, there are the technical limitations that we would like to improve in the future. The spectral bandwidth in the current device is limited in exchange for large imaging depth for better alignment. With our new linear-K spectrometer design and extended imaging depth (31), the spectral bandwidth can be increased to improve the robustness and accuracy of sO$_2$ calculation.

In summary, we investigated parafoveal microvascular sO$_2$ using VIS-OCT on healthy subjects in this initial baseline study. The statistical analysis reveals that no significant association between sO$_2$ and vessel topographic features. Also, there are no significant correlations for the eye sO$_2$ and clinical parameters except the relation of VsO$_2$ and IOP, CDR and age. This study will provide a normal (an initial) database for later sO$_2$ investigations in ocular diseases.

DATA AVAILABILITY STATEMENT

The raw data supporting the conclusions of this article will be made available by the authors, without undue reservation.

ETHICS STATEMENT

The studies involving human participants were reviewed and approved by Boston Medical Center. The patients/participants provided their written informed consent to participate in this study.

AUTHOR CONTRIBUTIONS

JY supervised this project. JW and JY analyzed the results. JW, WS, MF, MD, and JY contributed the manuscript. WS, NS, MF, and MD assisted in subject screening and recruitment. All authors contributed to the article and approved the submitted version.

FUNDING

SUPPLEMENTARY MATERIAL

The Supplementary Material for this article can be found online at: https://www.frontiersin.org/articles/10.3389/fmed.2022.886576/full#supplementary-material

REFERENCES

1. Stefánsson E, Olafsdottir OB, Eliasdottir TS, Vehmeijer W, Einarsdottir AB, Bek T, et al. Retinal oximetry: metabolic imaging for diseases of the retina and brain. *Prog Retin Eye Res.* (2019) 70:1–22. doi: 10.1016/j.preteyeres.2019.04.001

2. Whalen W, Riley J, Nair P. A microelectrode for measuring intracellular PO2. *J Appl Physiol.* (1967) 23:798–801. doi: 10.1152/jappl.1967.23.5.798

3. Olafsdottir OB, Hardarson SH, Gottfredsdottir MS, Harris A, Stefánsson E. Retinal oximetry in primary open-angle glaucoma. *Invest Ophthalmol Vis Sci.* (2011) 52:6409–13. doi: 10.1167/iovs.10-6985

4. Hardarson SH, Stefánsson E. Retinal oxygen saturation is altered in diabetic retinopathy. *Br J Ophthalmol.* (2012) 96:560–3. doi: 10.1136/bjophthalmol-2011-300640

5. Hardarson SH, Stefánsson E. Oxygen saturation in central retinal vein occlusion. *Am J Ophthalmol.* (2010) 150:871–5. doi: 10.1016/j.ajo.2010.06.020

6. Geirsdottir A, Hardarson SH, Olafsdottir OB, Stefánsson E. Retinal oxygen metabolism in exudative age-related macular degeneration. *Acta ophthalmologica.* (2014) 92:27–33. doi: 10.1111/aos.12294

7. Hardarson SH, Harris A, Karlsson RA, Halldorsson GH, Kagemann L, Rechtman E, et al. Automatic retinal oximetry. *Invest Ophthalmol Vis Sci.* (2006) 47:5011–6. doi: 10.1167/iovs.06-0039

8. Yi J, Wei Q, Liu W, Backman V, Zhang HF. Visible-light optical coherence tomography for retinal oximetry. *Opt Lett.* (2013) 38:1796–8. doi: 10.1364/OL.38.001796

9. Chong SP, Bernucci M, Radhakrishnan H, Srinivasan VJ. Structural and functional human retinal imaging with a fiber-based visible light OCT ophthalmoscope. *Biomed Opt Express.* (2017) 8:323–37. doi: 10.1364/BOE.8.000323

10. Pi S, Camino A, Zhang M, Cepurna W, Liu G, Huang D, et al. Angiographic and structural imaging using high axial resolution fiber-based visible-light OCT. *Biomed Opt Express.* (2017) 8:4595–608. doi: 10.1364/BOE.8.004595

11. Shu X, Beckmann LJ, Zhang HF. Visible-light optical coherence tomography: a review. *J Biomed Opt.* (2017) 22:121707. doi: 10.1117/1.JBO.22.12.121707

12. Yi J, Chen S, Shu X, Fawzi AA, Zhang HF. Human retinal imaging using visible-light optical coherence tomography guided by scanning laser ophthalmoscopy. *Biomed Opt Express.* (2015) 6:3701–13. doi: 10.1364/BOE.6.003701

13. Robles FE, Wilson C, Grant G, Wax A. Molecular imaging true-colour spectroscopic optical coherence tomography. *Nature photonics.* (2011) 5:744–7. doi: 10.1038/nphoton.2011.257

14. Wang J, Baker A, Subramanian ML, Siegel NH, Chen X, Ness S, et al. Simultaneous visible light optical coherence tomography and near infrared

OCT angiography in retinal pathologies: a case study. *Exp Biol Med.* (2021) 247:377–84. doi: 10.1177/15353702211063839

15. Ghassabi Z, Tayebi B, Wu M, Palmer S, Zambrano R, Li J, et al. Retinal oximetry revealed glaucomatous eyes had lower retinal metabolism using Visible Light Optical Coherence Tomography (vis-OCT). *Invest Ophthalmol Vis Sci.* (2021) 62:2526.

16. Kfir J, Ghassabi Z, Wu M, Rubinoff I, Kuranov RV, Wang Y, et al. Visible-Light OCT captures *in-vivo* changes in retinal oximetry in ischemic retinal diseases. *Invest Ophthalmol Vis Sci.* (2020) 61:PB00111.

17. Curcio CA, Allen KA. Topography of ganglion cells in human retina. *J Comp Neurol.* (1990) 300:5–25. doi: 10.1002/cne.903000103

18. Yoneya S, Saito T, Nishiyama Y, Deguchi T, Takasu M, Gil T, et al. Retinal oxygen saturation levels in patients with central retinal vein occlusion. *Ophthalmology.* (2002) 109:1521–6. doi: 10.1016/S0161-6420(02)01109-0

19. Olafsdottir OB, Vandewalle E, Pinto LA, Geirsdottir A, De Clerck E, Stalmans P, et al. Retinal oxygen metabolism in healthy subjects and glaucoma patients. *Br J Ophthalmol.* (2014) 98:329–33. doi: 10.1136/bjophthalmol-2013-303162

20. Hardarson SH, Stefánsson E. Oxygen saturation in branch retinal vein occlusion. *Acta Ophthalmol.* (2012) 90:466–70. doi: 10.1111/j.1755-3768.2011.02109.x

21. Chylack LT, Leske MC, McCarthy D, Khu P, Kashiwagi T, Sperduto R. Lens opacities classification system II (LOCS II). *Arch Ophthalmol.* (1989) 107:991–7. doi: 10.1001/archopht.1989.01070020053028

22. Song W, Shao W, Yi W, Liu R, Desai M, Ness S, et al. Visible light optical coherence tomography angiography (vis-OCTA) facilitates local microvascular oximetry in the human retina. *Biomed Opt Express.* (2020) 11:4037–51. doi: 10.1364/BOE.395843

23. Bradley D, Roth G. Adaptive thresholding using the integral image. *J Graph Tools.* (2007) 12:13–21. doi: 10.1080/2151237X.2007.10129236

24. Geirsdottir A, Palsson O, Hardarson SH, Olafsdottir OB, Kristjansdottir JV, Stefánsson E. Retinal vessel oxygen saturation in healthy individuals. *Invest Ophthalmol Vis Sci.* (2012) 53:5433–42. doi: 10.1167/iovs.12-9912

25. Jani PD, Mwanza J-C, Billow KB, Waters AM, Moyer S, Garg S. Normative values and predictors of retinal oxygen saturation. *Retina.* (2014) 34:394–401. doi: 10.1097/IAE.0b013e3182979e7b

26. Bata AM, Fondi K, Szegedi S, Aschinger GC, Hommer A, Schmidl D, et al. Age-related decline of retinal oxygen extraction in healthy subjects. *Invest Ophthalmol Vis Sci.* (2019) 60:3162–9. doi: 10.1167/iovs.18-26234

27. Liu X, He X, Yin Y, Zhang B, Sun S, Zhu J, et al. Retinal oxygen saturation in 1461 healthy children aged 7–19 and its associated factors. *Acta ophthalmologica.* (2019) 97:287–95. doi: 10.1111/aos.14043

28. Nomura H, Ando F, Niino N, Shimokata H, Miyake Y. The relationship between age and intraocular pressure in a Japanese population: the influence of central corneal thickness. *Curr Eye Res.* (2002) 24:81–5. doi: 10.1076/ceyr.24.2.81.8161

29. Vandewalle E, Abegao Pinto L, Olafsdottir OB, De Clerck E, Stalmans P, Van Calster J, et al. Oximetry in glaucoma: correlation of metabolic change with structural and functional damage. *Acta Ophthalmol.* (2014) 92:105–10. doi: 10.1111/aos.12011

30. Ashman RA, Reinholz F, Eikelboom RH. Oximetry with a multiple wavelength SLO. *Int Ophthalmol.* (2001) 23:343–6. doi: 10.1023/A:1014406831412

31. Song W, Shao W, Yi J, editors. *Wide-Field and Micron-Resolution Visible Light Optical Coherence Tomography in Human Retina by a Linear-K Spectrometer.* Bio-Optics: Design and Application (2021) Optical Society of America. doi: 10.1364/BODA.2021.DM2A.4